Assessing the SMOS Soil Moisture Retrieval Parameters With High-Resolution NAFE'06 Data

O. Merlin, J.P. Walker, R. Panciera, M.-J. Escorihuela, T.J. Jackson

Assessing the SMOS Soil Moisture Retrieval Parameters With High-Resolution NAFE'06 Data

Olivier Merlin, Jeffrey Phillip Walker, Rocco Panciera, Maria José Escorihuela, and Thomas J. Jackson

***Abstract*—The spatial and temporal invariance of Soil Moisture and Ocean Salinity (SMOS) forward model parameters for soil moisture retrieval was assessed at 1-km resolution on a diurnal basis with data from the National Airborne Field Experiment 2006. The approach used was to apply the SMOS default parameters uniformly over 27 1-km validation pixels, retrieve soil moisture from the airborne observations, and then to interpret the differences between airborne and ground estimates in terms of land use, parameter variability, and sensing depth. For pastures (17 pixels) and nonirrigated crops (5 pixels), the root mean square error (rmse) was 0.03 volumetric (vol./vol.) soil moisture with a bias of 0.004 vol./vol. For pixels dominated by irrigated crops (5 pixels), the rmse was 0.10 vol./vol., and the bias was −0.09 vol./vol. The correlation coefficient between bias in irrigated areas and the 1-km field soil moisture variability was found to be 0.73, which suggests either 1) an increase of the soil dielectric roughness (up to about one) associated with small-scale heterogeneity of soil moisture or/and 2) a difference in sensing depth between an L-band radiometer and the *in situ* measurements, combined with a strong vertical gradient of soil moisture in the top 6 cm of the soil.**

***Index Terms*—Airborne experiment, calibration, L-band radiometry, National Airborne Field Experiment (NAFE), retrieval algorithm, soil moisture, Soil Moisture and Ocean Salinity (SMOS).**

I. Introduction

THE SOIL Moisture and Ocean Salinity (SMOS, [1]) retrieval algorithm for soil moisture is based on an L-band emission (forward) model calibrated for different soil and vegetation classes [2], [3]. The main parameters involved in the model are the near-surface soil moisture, soil texture, soil surface roughness, soil effective temperature, and vegetation optical depth. In the SMOS level 2 processor [4], brightness temperature is simulated at a 1–4-km resolution by the forward model (land use and land cover are assumed to be uniform at 1–4-km resolution), aggregated to the SMOS observation scale (∼40 km), and then compared with the SMOS observed brightness temperature. The angular and polarization capabilities of the SMOS antenna will allow retrieval of several additional parameters (e.g., vegetation optical depth and soil roughness). However, the performance of multiparameter retrieval approaches [5] depends on how well the parameters bounds are estimated, i.e., *a priori* knowledge of minimum and maximum values. Retrieval assumes that the parameters are rather stable at 1–4-km resolution. However, few experiments have provided multiple angle and polarization L-band data at the intermediate resolution of ∼1 km to verify this assumption.

One objective of the National Airborne Field Experiment 2006 (NAFE'06) was to map L-band brightness temperature at 1-km resolution over a range of surface conditions including grassland (pasture and fallow), dry land cropping (wheat, barley, and oats) and irrigated cropping (wheat, alfalfa, canola, rice, and corn) [6]. During NAFE'06, ground measurements of the 0–6-cm soil moisture were made coincident with 1-km resolution flights on ten days during the three-week campaign that included two rainfall events of about 7 and 13 mm. NAFE'06 provided a unique data set to test the spatial invariance of retrieval parameters over various land uses, vegetation covers, and surface conditions at 1-km resolution. The approach used was to apply SMOS default parameters uniformly over 27 1-km validation pixels, retrieve surface soil moisture from the airborne observations, and then to interpret differences between airborne and ground estimates in terms of land use, parameter variability, and sensing depth.

II. L-Band Emission Model

The SMOS forward model is based on the L-band Microwave Emission of the Biosphere model described in [2]. It includes the tau-omega formulation [7] to express the polarized (H or V) brightness temperature as a function of incidence angle, soil effective temperature, soil emissivity, and nadir optical depth (τ) and single-scattering albedo (ω) of the canopy. The soil microwave emissivity is calculated using the incidence angle, the Fresnel equations, and the soil dielectric permittivity that is computed using the Dobson model [8] and ancillary soil texture. The soil roughness is accounted for using the approach described in [9], which is based on two best fit parameters H and Q. The nadir optical depth τ is related to vegetation water content (VWC) by $\tau = b \times \mathrm{VWC}$ [10] with b a coefficient that is generally obtained from field measurements. In this letter, only the H-polarization (and H-polarized parameters) will be considered.

Since the main objective of this letter is to assess the stability of SMOS forward model parameters at a 1-km resolution, the SMOS default parameters were used. The soil effective temperature was computed based on the parameterization of [11] using soil temperature in the 0–5-cm soil layer, deep soil temperature (50 cm), and the default parameter values presented in [2]. The effects of temperature gradients within the

Manuscript received June 10, 2008; revised October 21, 2008 and December 4, 2008.

O. Merlin is with the Centre d'Etudes Spatiales de la Biosphère, 31401 Toulouse, France.

J. P. Walker and R. Panciera are with the Department of Civil and Environmental Engineering, The University of Melbourne, Melbourne, Vic. 3010, Australia.

M. J. Escorihuela is with IsardSAT, 08031 Barcelona, Spain.

T. J. Jackson is with the U.S. Department of Agriculture, Annapolis, MD 21409-5543 USA.

Digital Object Identifier 10.1109/LGRS.2008.2012727

TABLE I
MEAN 1-km FIELD VARIABILITY OF GROUND MEASUREMENTS AND RMSE, CORRELATION COEFFICIENT, SLOPE OF THE LINEAR REGRESSION, AND MEAN DIFFERENCE (BIAS) BETWEEN 1-km RESOLUTION RETRIEVALS AND 1-km FIELD AVERAGES FOR EACH OF THE 27 VALIDATION PIXELS. THE NUMBER OF SAMPLING DAYS IS ALSO LISTED

Pixel label	Main land use	Main land cover	Variability (vol./vol.)	RMSE (vol./vol.)	Correlation coefficient	Regression slope	Bias (% vol.)	Number of days
Y2a	grazing	grass	0.026	0.035	0.87	0.87	0.007	10
Y2b	grazing	grass	0.031	0.026	0.94	1.0	0.014	10
Y2c	grazing	grass	0.030	0.034	0.91	0.83	0.017	10
Y2d	grazing	grass	0.035	0.042	0.83	1.1	0.005	10
Y2e	grazing	grass	0.036	0.043	0.79	0.78	−0.008	10
Y2f	grazing	grass	0.038	0.034	0.87	0.88	0.031	10
Y2g	grazing	grass	0.041	0.034	0.92	1.2	0.008	10
Y2h	grazing	grass	0.040	0.030	0.92	1.0	0.009	10
Y2i	grazing	grass	0.042	0.023	0.94	0.89	0.004	10
Y9a	fallow	grass	0.034	0.034	0.72	0.41	0.004	10
Y9b	fallow	grass	0.025	0.024	0.90	0.74	0.012	9
Y9c	grazing	grass	0.030	0.028	0.90	1.3	−0.012	8
Y9d	cropping/grazing	alfalfa	0.068	0.027	0.75	0.43	0.001	10
Y9e	cropping	oats/barley	0.032	0.032	0.89	0.48	0.003	10
Y9f	grazing	grass	0.044	0.026	0.84	0.75	0.003	10
Y9g	cropping*	alfalfa	0.098	0.10	0.92	0.50	−0.090	10
Y9h	cropping	grass	0.059	0.042	0.85	0.58	0.022	10
Y9i	cropping	grass	0.032	0.023	0.92	0.72	−0.006	10
Y12a	cropping*	wheat	0.033	0.056	0.85	0.52	−0.044	8
Y12b	grazing	grass	0.029	0.027	0.89	0.80	−0.007	8
Y12c	grazing	grass	0.027	0.037	0.81	0.95	0.007	8
Y12d	cropping*	wheat	0.13	0.14	0.68	0.47	−0.13	10
Y12e	cropping*	canola	0.11	0.12	0.75	0.80	−0.11	10
Y12f	grazing	grass	0.035	0.043	0.78	0.87	0.005	10
Y12g	cropping*	cut corn	0.090	0.089	0.86	0.93	−0.086	9
Y12h	grazing	grass	0.064	0.051	0.63	0.46	−0.017	10
Y12i	grazing	grass	0.083	0.033	0.87	0.82	−0.012	10

* includes at least one crop that was irrigated during NAFE'06.

canopy were assumed to be minimal by assuming the vegetation temperature throughout the canopy is equal to the near-surface soil temperature. The soil roughness parameter H was set to 0.1 and the polarization-mixing parameter Q to 0 [2]. The b parameter was set to a value 0.15, which is representative of most agricultural crops [10], and the single scattering albedo ω to 0.05 [2]. Water interception in vegetation was assumed to be negligible. Note that one pixel included 20% of rice under flood irrigation. The contribution of standing water was removed from the total emission by simulating the L-band emission over water as a function of surface water temperature and incidence angle [12].

III. DATA

NAFE'06 was undertaken during three weeks in November 2006 over a 40 by 60 km area in southeastern Australia $(-34.9^\circ\ \mathrm{N}; 146.1^\circ\ \mathrm{E})$. In this letter, the study area is composed of 27 1-km resolution pixels included in three farms noted as Y2, Y9, and Y12. Land use and land cover are listed in Table I. Within each 1-km area, the 0–6-cm soil moisture was measured on a 250-m resolution grid using a Hydraprobe. An average of three successive measurements ∼1 m apart was made at each node of the sampling grid, resulting in about 50 measurements within each 1-km pixel. Note that the calibration equation that was applied to all measurements is site specific [13].

TABLE II
MEAN AND STANDARD DEVIATION OF 0–6-cm SOIL MOISTURE, H-POLARIZED BRIGHTNESS TEMPERATURE, AND NEAR-SURFACE SOIL TEMPERATURE FOR EACH OF THE TEN SAMPLING DAYS AT TIME OF AIRCRAFT OVERPASS. TWO RAINFALL EVENTS OCCURRED DURING THE THREE-WEEK CAMPAIGN WITH ∼7 mm ON JD 306-307 AND ∼13 mm ON JD 316-317

	Mean (standard deviation)		
JD	soil moisture (vol./vol.)	brightness temperature (K)	soil temperature (°C)
304	0.051 (0.053)	266 (7.7)	41 (7.0)
306	0.057 (0.058)	269 (7.7)	36 (2.4)
308	0.11 (0.075)	246 (7.8)	39 (1.2)
309	0.085 (0.063)	259 (8.8)	39 (1.3)
311	0.078 (0.067)	266 (8.0)	38 (6.0)
313	0.059 (0.056)	267 (8.1)	39 (1.4)
317	0.22 (0.055)	216 (13)	29 (5.7)
318	0.18 (0.047)	240 (9.5)	31 (4.8)
320	0.16 (0.055)	243 (11)	22 (6.0)
322	0.098 (0.040)	263 (9.9)	44 (1.1)

Concurrently with ground observations, the H- and V-polarized brightness temperature was measured at 1-km resolution by the airborne Polarimetric L-band Multibeam Radiometer (PLMR). Flights were undertaken in the window 8:00 A.M.–10:30 A.M. on Julian day (JD) 304, 306, 308,

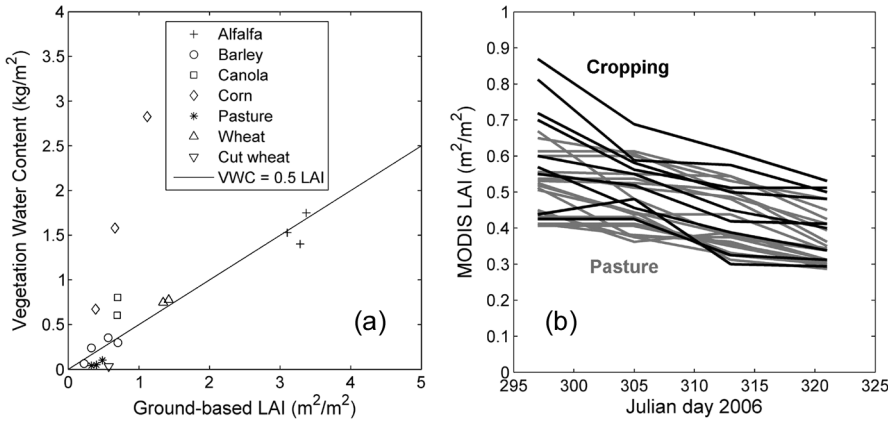

Fig. 1. (Left) Ground-based measurement of VWC versus LAI for each vegetation type in the study area, and (right) time series of MODIS eight-day LAI product extracted for each 1-km pixel.

309, 311, 313, 320, and 322 and in the window 11:00 A.M.–1:30 P.M. on JD 317 and 318. The same flight lines were kept across the campaign to obtain approximately the same incidence angle over each pixel. Note that changes in aircraft attitude were accounted for during processing by correcting the zero tilt and roll incidence angle of the six beams (which are $\pm 7^\circ$, $\pm 21.5^\circ$, $\pm 38.5^\circ$) with respect to the topography. Details about PLMR and its calibration can be found in [14]. Some minor occurrences of sunglint were detected in the NAFE'06 area, but not over the sampling areas [15].

To compare ground and airborne observations, the point-scale soil moisture measurements were averaged at 1-km resolution within each of the 27 validation pixels. The along track 1-km resolution radiometric measurements (together with incidence angle) were also averaged within each 1-km pixel. Note that the mean number of PLMR acquisitions along a 1-km run was about 30 (with a time step of about 1.5 s and an aircraft speed of 200 km/h). During the three-week experiment, the mean soil moisture ranged from about 0.05 to 0.20 vol./vol. corresponding to a mean brightness temperature of 270 K and 220 K, respectively (see Table II).

VWC was estimated from MODIS/Terra 1-km resolution eight-day LAI products on JD 297, 305, 313, and 312 using the relationship VWC $= 0.5$ LAI [16]. VWC maps were then linearly interpolated between dates and regridded on the same 1-km grid as processed PLMR brightness temperature. The relationship between VWC and LAI during NAFE'06 is shown in Fig. 1(a) using ground observations obtained during the campaign. The slope 0.5 appears to hold for all vegetation types encountered except for corn, which has a slope of about three. However, there was very little corn in the study area. The time series of MODIS LAI for grazing and cropping pixels is shown in Fig. 1(b). At 1-km resolution, LAI ranged from 0.4 to 0.8 and generally decreased by about 0.1 during the three-week experiment.

To compute effective soil temperature, near-surface soil temperature was estimated by the MODIS/Terra 1-km resolution daily temperature on clear sky days (JD 304, 309, 311, 313, 318, 320, and 322) and by the average of the 12 (six stations distributed in the study area with two replicates per station) simultaneous -1-cm soil temperature measurements on cloudy days (JD 306, 308, and 317). Note that the mean ground soil temperature was extracted for each pixel at the time of aircraft overflight (ranging from 8:30 A.M. to 12:30 A.M.). Table II presents the time series of the mean and standard deviation of near-surface soil temperature. Soil temperature at 50-cm depth was also estimated from permanent monitoring stations in the study region.

Soil texture was analyzed for 12 0–5-cm soil samples collected in the study area. The mean and standard deviation of sand and clay fractions were estimated as 0.26 ± 0.10 and 0.27 ± 0.11, respectively. The highest measured sand fraction was 0.59 (with a clay fraction of 0.11) and the highest clay fraction was 0.49 (with a sand fraction of 0.11). In this letter, the sand and clay fractions are assumed to be uniform and set to 0.3.

Soil surface roughness was measured with a pin profiler at five locations within each farm. As the link between the measured geometrical roughness and H parameter is not well known [2], those measurements were not used in this letter.

IV. Retrieval Results

Airborne soil moisture was retrieved by minimizing a cost function. This cost function is defined as the root mean square difference between the H-polarized brightness temperature modeled by the radiative transfer model and that observed by the aircraft. All parameters were uniformly set to the values presented above, i.e., soil moisture was the only free parameter in the minimization. The V-polarized brightness temperature was not included in the cost function to simplify the interpretation of retrieval results due to the uncertainty of polarization dependence on the parameters (e.g., roughness). Note that the retrieval was done at the 1-km resolution and the effects of mixed surface in the 1-km resolution footprint were not accounted for except in the presence of standing water.

Fig. 2 compares the 1-km field soil moisture average (cross) and variability (whisker) with the soil moisture retrieval for farms Y2, Y9, and Y12. The 1-km field variability of soil moisture was computed as the standard deviation of the ground measurements within the 1-km PLMR pixel. In most cases, the difference between ground measurements and airborne estimates was smaller than the 1-km field variability (see Table I). However, a significant bias was apparent for the five irrigated pixels (labeled Y9g, Y12a,d,e,g), although only one pixel (Y9g) contained a measurable fraction (20%) of standing water. Table I lists for each of the 27 validation pixels the root

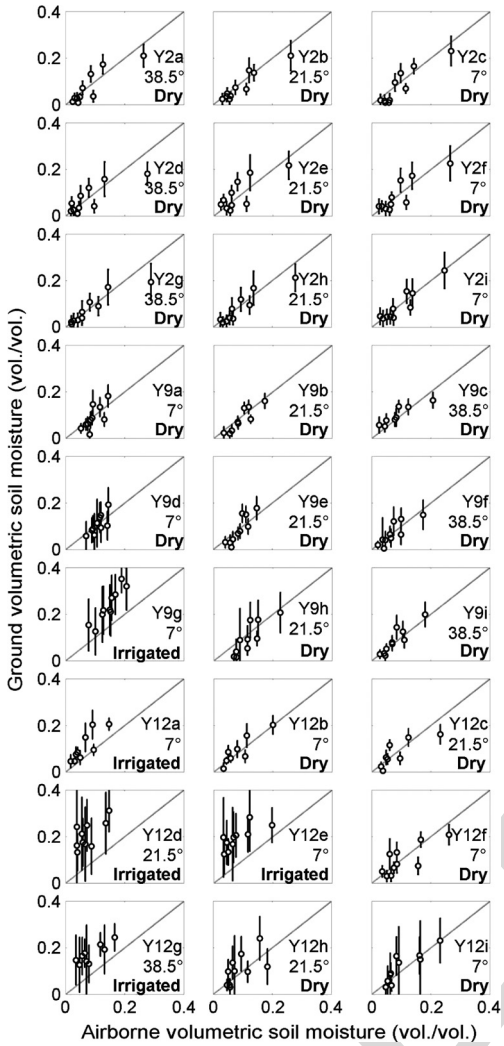

Fig. 2. One-kilometer (cross) field average and (whisker) variability of *in situ* measurements versus retrievals at the 27 1-km resolution validation pixels. Pixel label and mean incidence angle are also indicated.

mean square error (rmse), the correlation coefficient, and the bias between airborne retrievals and ground measurements. For the 22 nonirrigated pixels, the rmse is 0.033 ($\pm$0.009) vol./vol. with a correlation coefficient of 0.85 ($\pm$0.07) and a bias of 0.004 ($\pm$0.010) vol./vol. when using the SMOS default parameters. For the five irrigated pixels, the rmse is 0.10 ($\pm$0.032) vol./vol. with a correlation coefficient of 0.81 ($\pm$0.10) and a bias of -0.093 ($\pm$0.034) vol./vol.

The bias observed for the airborne soil moisture estimates in the five irrigated pixels could be explained by several factors: The spatial variability of soil texture, soil roughness and/or vegetation. First, soil texture (i.e., sand and clay fractions) impacts the modeled soil emissivity, which in turn impacts the retrieved soil moisture. However, when using the parameters of the soil with the highest measured sand fraction and then those with the highest measured clay fraction in the retrieval algorithm (results not shown), the root mean square difference between the two output data sets was only 0.027 vol./vol., which is much smaller than the observed bias (0.09 vol./vol.).

Soil geometric roughness impacts the slope of the relationship between soil moisture retrievals and ground measurements. In order to assess the variability of soil geometric roughness at 1-km resolution, we examined the slope of the linear regression between airborne and ground estimates (Table I). The slope is 0.87 $\pm$ 0.21 for grazing pixels, 0.56 $\pm$ 0.13 for dry land cropping pixels, and 0.65 $\pm$ 0.20 for irrigated cropping pixels. The difference in the slopes between the grazing and cropping classes was associated with an increase in roughness with agricultural practices in cropped fields (e.g., plowing, irrigation rows, etc.). However, no significant difference in the slopes was observed between the irrigated and nonirrigated areas. Consequently, soil geometric roughness is not considered to be the main cause of the bias observed in the irrigated pixels.

The last factor considered was vegetation. The different effects (attenuation, scattering and emission) of vegetation at L-band generally result in an increase of the surface emission. An increase of vegetation optical depth would thus make the soil moisture retrieval lower. However, vegetation cannot explain a 0.09 vol./vol. decrease in retrieved soil moisture because vegetation cover was relatively low at 1-km resolution (LAI ranged from 0.4 to 0.8). Moreover, the b parameter was fixed in the higher range for crops (0.05–0.20), which already maximizes the vegetation impact on the modeled brightness temperature. As an illustration, the irrigated canola in Y12e was harvested during the middle of the campaign, but harvesting did not remove the bias on retrievals (see Fig. 2).

If none of the parameters of the L-band emission model can provide an obvious explanation of the bias found for the airborne estimates, then one may argue that perhaps the ground sensor calibration is not valid in irrigated areas. Four out of the five irrigated pixels are located in the most clayey farm Y12, and it is known that clay fraction can potentially increase the ground sensor response [13]. However, soil type was similar at the farm scale, and no significant bias was observed for the five nonirrigated pixels of Y12 (see Fig. 2). Consequently, the calibration of the ground sensor, which mainly depends on soil type, is considered to be reliable for irrigated areas as well.

Having considered the uncertainty in retrieval model inputs and ground measurement data, it was concluded that the poor retrieval results in irrigated areas was due to either a difference in sensing depth between ground and airborne measurements and/or an error in the modeling of soil roughness. The first hypothesis was to consider the different depths of soil involved in the direct and remote measurements. During or immediately after irrigation, the soil moisture of the first layer sensed by the L-band radiometer (0–3 cm according to [17]) could be different to the soil moisture of the lower layer (3–6 cm) that instead affects the soil moisture measurements carried out by using 0–6-cm Hydraprobes. This hypothesis is supported by the relatively high correlation (estimated to 0.73) between the bias on retrievals and the 1-km field soil moisture variability [see Fig. 3(a)]. However, no information on the soil moisture profile in the top 6 cm was available to confirm the link between vertical and horizontal variability. The second hypothesis was to consider an increase of the "dielectric roughness" with the variability of moisture within the soil. To illustrate the possible impact of the soil moisture variability on soil dielectric roughness, parameter H was retrieved in the four irrigated pixels of Y12 by setting soil moisture to ground measurements. Fig. 3(b) shows that the retrieved effective roughness does increase (up to about one) as a function of the 1-km field soil moisture variability with a correlation coefficient estimated to 0.67.

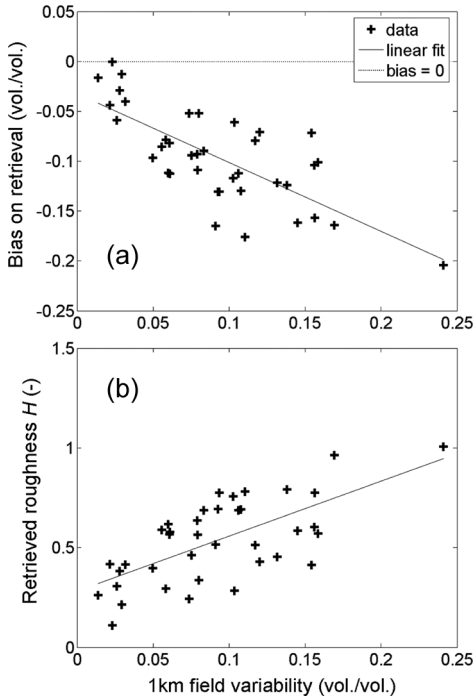

Fig. 3. Difference between (a) airborne and ground estimates and (b) retrieved soil roughness parameter H versus 1-km field soil moisture variability including data from the four irrigated pixels in Y12.

V. Conclusion

The temporal and spatial invariance of the SMOS forward model parameters was assessed at a 1-km resolution on a diurnal basis using the NAFE'06 data. The approach used was to apply the SMOS default parameters uniformly over 27 1-km pixels, retrieve soil moisture from the airborne observations, and then to interpret differences between airborne and ground estimates in terms of land use, parameter variability, and sensing depth. For nonirrigated (grazing and cropping) areas, the rmse on retrievals was 0.03 vol./vol. and the correlation coefficient with ground measurements was 0.85. The impact of soil geometric roughness was noted by correlating the slope of the linear regression between airborne and ground estimates with agricultural practices. A roughness parameter $H = 0.1$ was found to be appropriate for grazing areas (slope was about one), while a slightly higher roughness was identified for cropping areas (slope was about 0.7). A significant mean difference of -0.09 vol./vol. between airborne and ground estimates was observed in the five irrigated pixels. As no parameter (soil texture, soil geometric roughness, vegetation) could explain this bias, it is suggested that either a strong vertical gradient of near-surface soil moisture in irrigated areas made the 0–6-cm ground measurements generally wetter than the 0–3-cm retrievals and/or the small-scale variability of soil moisture made the effective soil roughness increase up to about one.

Acknowledgment

The authors would like to thank the NAFE'06 participants. The NAFEs have been made possible through recent infrastructure (LE0453434 and LE0560930) and research (DP0557543) funding from the Australian Research Council, and the collaboration of a large number of scientists from throughout Australia, U.S., and Europe. Initial setup and maintenance of the study catchments was funded by a research Grant (DP0343778) from the Australian Research Council and by the Cooperative Research Centre for Catchment Hydrology.

References

[1] Y. H. Kerr, P. Waldteufel, J.-P. Wigneron, J.-M. Martinuzzi, J. Font, and M. Berger, "Soil moisture retrieval from space: The soil moisture and ocean salinity (SMOS) mission," *IEEE Trans. Geosci. Remote Sens.*, vol. 39, no. 8, pp. 1729–1735, Aug. 2001.

[2] J.-P. Wigneron, Y. Kerr, P. Waldteufel, K. Saleh, M.-J. Escorihuela, P. Richaume, P. Ferrazzoli, P. de Rosnay, R. Gurneye, J.-C. Calvet, J. P. Grant, M. Guglielmettih, B. Hornbuckle, C. Matzler, T. Pellarin, and M. Schwank, "L-band microwave emission of the biosphere (L-MEB) Model: Description and calibration against experimental data sets over crop fields," *Remote Sens. Environ.*, vol. 107, no. 4, pp. 639–655, Apr. 2007.

[3] K. Saleh, J.-P. Wigneron, P. Waldteufel, P. de Rosnay, M. Schwank, J.-C. Calvet, and Y. H. Kerr, "Estimates of surface soil moisture under grass covers using L-band radiometry," *Remote Sens. Environ.*, vol. 109, no. 1, pp. 42–53, Jul. 2007.

[4] Y. H. Kerr, P. Waldteufel, P. Richaume, I. Davenport, P. Ferrazzoli, and J.-P. Wigneron, *SMOS Level 2 Processor Soil Moisture Algorithm Theoretical Basis Document (ATBD)*. Toulouse, France: CESBIO, 2006. SM-ESL (CBSA), vol. SO-TN-ESL-SM-GS-0001, V5.a..

[5] M. Parde, J.-P. Wigneron, P. Waldteufel, Y. H. Kerr, A. Chanzy, S. S. Sobjaerg, and N. Skou, "N-parameter retrievals from L-band microwave observations acquired over a variety of crop fields," *IEEE Trans. Geosci. Remote Sens.*, vol. 42, no. 6, pp. 1168–1178, Jun. 2004.

[6] O. Merlin, J. P. Walker, J. D. Kalma, E. J. Kim, J. Hacker, R. Panciera, R. Young, G. Summerell, J. Hornbuckle, M. Hafeez, and T. J. Jackson, "The NAFE'06 data set: Towards soil moisture retrieval at intermediate resolution," *Adv. Water Resour.*, vol. 31, no. 11, pp. 1444–1455, Nov. 2008. DOI: 10.1016/j.advwatres.2008.01.018..

[7] T. Mo, B. J. Choudhury, T. J. Schmugge, J. R. Wang, and T. J. Jackson, "A model for microwave emission from vegetation-covered fields," *J. Geophys. Res.*, vol. 87, no. 13, pp. 11 229–11 237, 1982.

[8] M. C. Dobson, F. T. Ulaby, M. T. Hallikainen, and M. A. El-Reyes, "Microwave dielectric behavior of wet soil—Part II: Dielectric mixing models," *IEEE Trans. Geosci. Remote Sens.*, vol. GRS-23, no. 1, pp. 35–46, Jan. 1985.

[9] J. R. Wang and B. J. Choudhury, "Remote sensing of soil moisture content over bare field at 1.4 GHz frequency," *J. Geophys. Res.*, vol. 86, no. C6, pp. 5277–5282, Jun. 1981.

[10] T. J. Jackson and T. J. Schmugge, "Vegetation effects on the microwave emission of soils," *Remote Sens. Environ.*, vol. 36, no. 3, pp. 203–212, Jun. 1991.

[11] B. Choudhury, T. Schmugge, and T. Mo, "A parametrization of effective soil temperature for microwave emission," *J. Geophys. Res.*, vol. 87, no. C2, pp. 1301–1304, 1982.

[12] F. T. Ulaby, R. K. Moore, and A. K. Fung, *Microwave Remote Sensing: Active and Passive*, vol. 1. Norwood, MA: Artech House, 1981.

[13] O. Merlin, J. Walker, R. Panciera, R. Young, J. Kalma, and E. Kim, "Soil moisture measurement in heterogeneous terrain," in *Proc. Int. Congr. Model. Simul. MODSIM—Modelling and Simulation Society of Australia and New Zealand*, New Zealand, Dec. 2007, pp. 2604–2610.

[14] R. Panciera, J. P. Walker, J. D. Kalma, E. J. Kim, J. Hacker, O. Merlin, M. Berger, and N. Skou, "The NAFE'05/CoSMOS data set: Toward SMOS calibration, downscaling and assimilation," *IEEE Trans. Geosci. Remote Sens.*, vol. 46, no. 3, pp. 736–745, Mar. 2008. DOI: 10.1109/TGRS.2007.915403..

[15] M. J. Escorihuela, K. Saleh, P. Richaume, O. Merlin, J. P. Walker, and Y. Kerr, "Sunglint observations over land from ground and airborne L-band radiometer data," *Geophys. Res. Lett.*, vol. 35, no. 20, p. L20 406, Oct. 2008. DOI: 10.1029/2008GL035062.

[16] J.-P. Wigneron, A. Chanzy, J.-C. Calvet, A. Olioso, and Y. Kerr, "Modeling approaches to assimilating L-band passive microwave observations over land surfaces," *J. Geophys. Res.*, vol. 107, no. D14, pp. ACL 11.1–ACL 11.14, Jul. 2002. doi:10.1029/2001JD000958.

[17] S. Raju, A. Chanzy, J.-P. Wigneron, J.-C. Calvet, Y. Kerr, and L. Laguerre, "Soil moisture and temperature profile effects on microwave emission at low frequencies," *Remote Sens. Environ.*, vol. 54, no. 2, pp. 85–97, Nov. 2005.

AUTHOR QUERIES

AUTHOR PLEASE ANSWER ALL QUERIES

ATTN: If you are paying to have all or some of your figures appear in color in the print issue, it is very important that you fill out and submit a copy of the IEEE Page Charge & Reprint Form along with your proof corrections. This form is available from the same URL where these page proofs were downloaded from. Thank you.

END OF ALL QUERIES